ISSN 0016-7029, Geochemistry International, 2013, Vol. 51, No. 9, pp. 683–695. © Pleiades Publishing, Ltd., 2013.
Original Russian Text © E.A. Krasnova, M.V. Portnyagin, S.A. Silantyev, K. Hoernle, R. Werner, 2013, published in Geokhimiya, 2013, Vol. 51, No. 9, pp. 759–772.

# Two-Stage Evolution of Mantle Peridotites from the Stalemate Fracture Zone, Northwestern Pacific

**E. A. Krasnova[a], M. V. Portnyagin[a,b], S. A. Silantyev[a], K. Hoernle[b], and R. Werner[b]**

[a] *Vernadsky Institute of Geochemistry and Analytical Chemistry, Russian Academy of Sciences, ul. Kosygina 19, Moscow, 119991 Russia*
*e-mail: eakrasnova@gmail.com*

[b] *Helmholtz Center for Ocean Research Kiel (GEOMAR), Wischhofstr. 1–3, 24148 Kiel, Germany*

Received April 26, 2012; accepted July 19, 2012

**Abstract**—This paper reports the results of a mineralogical study of 14 mantle peridotite samples dredged in 2009 from the eastern slope of the northwestern segment of the Stalemate Ridge in the northwestern Pacific during cruise SO201-KALMAR Leg 1b of the R/V *Sonne*. The sample collection included four serpentinized and silicified dunites and ten variably serpentinized lherzolites. The compositions of primary minerals (clinopyroxene, orthopyroxene, and spinel) change systematically from the lherzolites to dunites. Spinel from the lherzolites shows higher Mg# and lower Cr# values (0.65–0.68 and 0.26–0.33, respectively) compared with spinel from the dunites (Mg# = 0.56–0.64 and Cr# = 0.38–0.43). Clinopyroxene from the lherzolites is less magnesian (Mg# = 91.7–92.4) than clinopyroxene from dunite sample DR37-3 (Mg# = 93.7). Based on the obtained data, it was concluded that the lherzolites of the Stalemate Fracture Zone were derived by 10–12% near-fractional melting of a DMM-type depleted mantle reservoir beneath the Kula–Pacific spreading center. The dunites were produced by interaction of residual lherzolites with sodium- and titanium-rich melt and are probably fragments of a network of dunite channels in the shallow mantle. The moderately depleted composition of minerals clearly distinguishes the lherzolites from the strongly depleted peridotites of the East Pacific Rise and indicates the existence of slow-spreading mid-ocean ridges in the Pacific Ocean during the Cretaceous–Paleogene.

***Keywords***: mantle peridotite, oceanic lithosphere, magmatism, partial melting

**DOI:** 10.1134/S0016702913080028

## INTRODUCTION

The nature of oceanic basement in the northwestern Pacific is still poorly known and remains a gap in our knowledge of the geological history of the Pacific Ocean. An important feature of this region is the preservation of a small fragment of the Kula plate, which was previously believed to have been entirely subducted. Pitman and Hayes [1] investigated the distribution of magnetic anomalies south of the Aleutian Trench and concluded that a relic of an ancient lithospheric plate, which migrated to the north faster than the Pacific plate, has preserved in this part of the northwestern Pacific. Grow and Atwater [2] assumed that this hypothetical plate had been entirely subducted and suggested the name Kula (from the Hawaiian, meaning "completely gone"). In the geodynamic context of the geologic history of the northwestern Pacific, it is similar to the Izanagi and Aluk (part of the Phoenix plate in the southeast) plates, which will completely disappear, according to [3], in the Aleutian subduction zone of eastern Asia and beneath the western margin of South America, respectively. Rea and Dixon [4] argued that the Kula plate was formed owing to the breakup of the Farallon plate during the formation of a Late Cretaceous rift zone. The newly formed crust of the Kula–Farallon plate was subsequently almost entirely subducted beneath North America, and the kinematics of the Kula–Pacific plate controlled the character of magnetic anomalies suitable for the dating of the basement of the northwestern Pacific [3]. According to paleomagnetic data, Kula–Pacific spreading ceased at approximately 43 Ma [3].

The last (not yet subducted) 75-km-long segment of the Kula Ridge adjoins the axis of the Aleutian Trench in the west-southwest at 171.5° E. A relic of the aforementioned paleo-spreading center of the Kula plate is bounded in the south by the Stalemate Fracture Zone, which is the northwestern end of the Kula–Pacific paleotransform fault and comprises an eponymous transverse ridge (Fig. 1). It is supposed that this ridge extending southeast–northwest for approximately 500 km was formed owing to the tectonic uplift of a block of oceanic lithosphere of Cretaceous (?) age along a transform fault [3]. However, there is still no data on the rocks of the Stalemate Ridge.

Cruise SO201 Leg 1b of the German R/V *Sonne* was conducted within the Russian–German KALMAR project in 2009 in the northwestern Pacific. It was focused, in particular, on the investigation of the Stalemate Fracture Zone. The results of multibeam bathim-

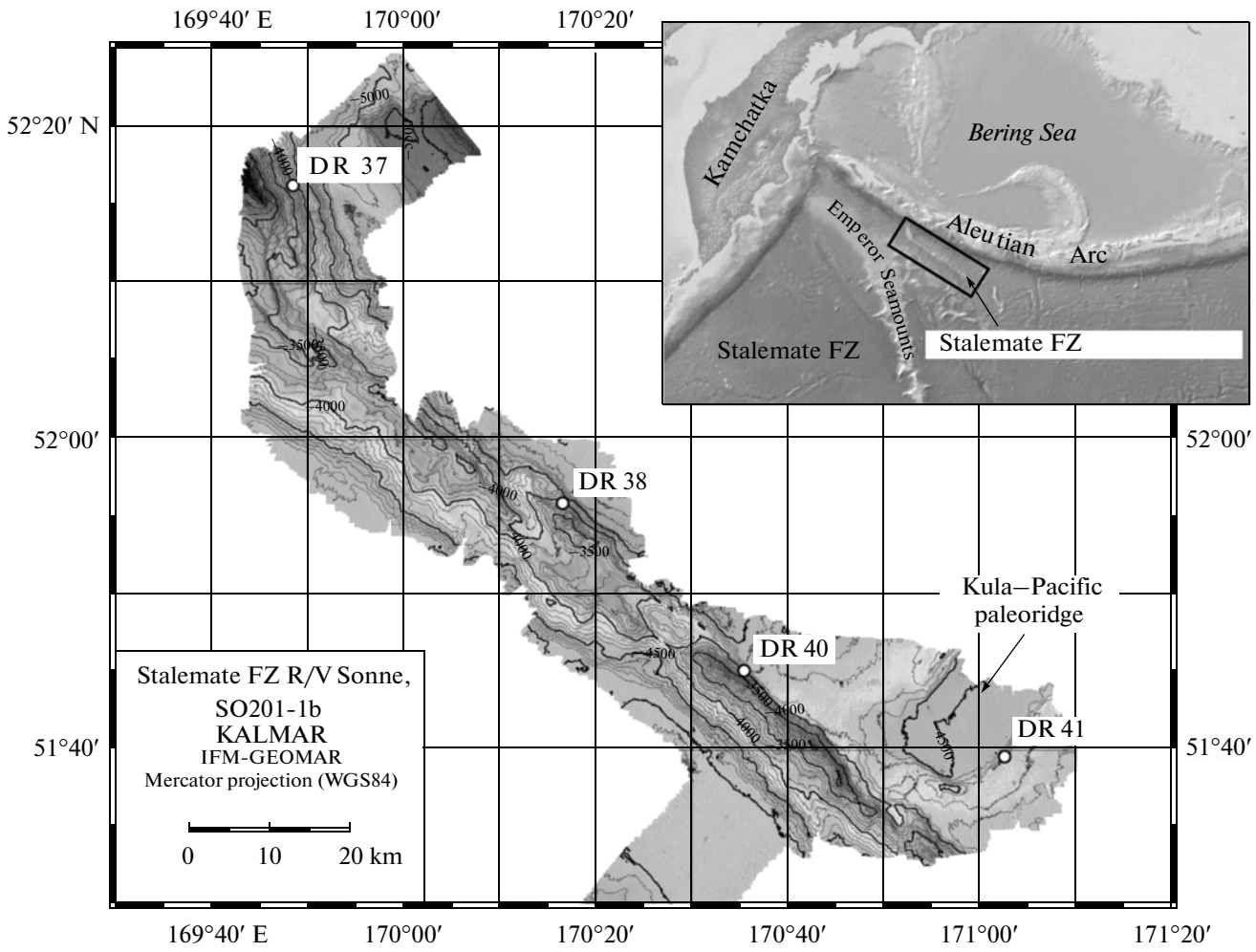


**Fig. 1.** Map of bottom topography and location of the dredging sites of the R/V *Sonne* at the region of the Stalemate paleo-transform fault. The peridotites discussed in this paper were dredged at station DR37 in the northwestern part of the ridge.

etry conducted during this cruise supported previous conclusions [3] and allowed unequivocal identification of this structure as a transverse ridge. Morphologically, the Stalemate Ridge is similar to transverse ridges extending parallel to adjacent transform faults in modern ocean basins and resulting from the tectonic uplift of the oceanic lithosphere along transform faults [5, 6]. Rocks dredged during the cruise at five stations along the Stalemate Ridge characterize the complete section of the oceanic lithosphere of the classic (Penrose) type, which was probably formed in the Kula–Pacific spreading center [7].

Variably altered mantle peridotites were dredged from the eastern slope of the northwestern segment of the Stalemate Ridge, where the ocean depth is 4600–3000 m. Dredging was carried out at depths of 4360–3955 m (Fig. 1). Among numerous rock fragments recovered at station SO201-1b-DR37, 13 representative samples of serpentinized lherzolites (nine samples) and strongly altered serpentinized silicified dunites (four samples) were collected. The bulk compositions of these samples and the character of their secondary alteration were reported elsewhere [8].

The goal of this study was to reconstruct the mantle stage of the compositional evolution of peridotites from the Stalemate Ridge. The microprobe analysis of relict primary minerals was the main tool.

## METHODS

Relicts of primary minerals were analyzed in double-polished thin sections and epoxy mounts (25 mm diameter) with monomineralic fractions 0.25–1.0 mm in grain size polished on one side. Major minerals were analyzed at the Helmholtz Center for Ocean Research (GEOMAR, Kiel, Germany) using a JEOL JXA 8200 electron microprobe equipped with five wavelength spectrometers, including high-sensitivity H-type spectrometers for the precise measurement of trace elements. Minerals were analyzed at an accelerating volt-

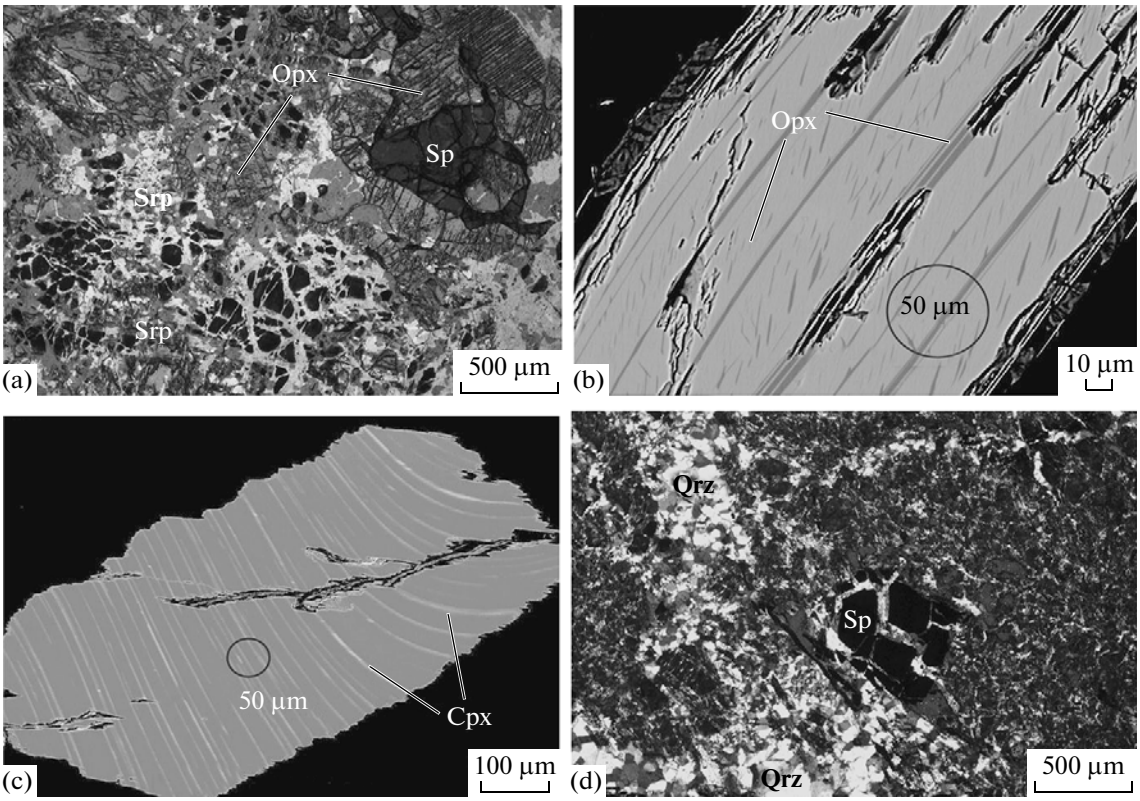


**Fig. 2.** Photomicrographs of serpentinized lherzolites from the Stalemate Fracture Zone. (a) Fragment of sample DR-37-9. The rock is 80% serpentinized, and former olivine core are completely replaced by serpentine. Parallel nicols, $D = 1.7$ mm. (b) Back-scattered electron image of a fragment of typical clinopyroxene from serpentinized lherzolite. Parallel orthopyroxene lamellae are seen over the whole grain area. Sample DR37-15. (c) Typical orthopyroxene from serpentinized lherzolite sample DR37-14. (d) Fragment of typical serpentinized and silicified dunite sample DR37-2. Serpentine is almost completely replaced by quartz. The degree of rock silicification is 70%. Parallel nicols, $D = 1.7$ mm. The diameter of electron beam (50 μm) is shown in Figs. 2b and 2c.

age of 15 kV and a beam current of 20 nA for pyroxenes and 50 nA for spinel. For local mineral analysis, the beam was focused to a spot of 1 μm. Clino- and orthopyroxenes containing low-temperature exsolution lamellae (Fig. 2) were analyzed with a 50 μm defocused beam for the estimation of their bulk compositions. Natural standards from the collection of Smithsonian Institute [9] were used for calibration. In order to check the quality of analysis, standard samples of pyroxene (USNM 12214 Kakanue Augite), chromite (USNM 117075), and ilmenite (USNM 96189) [9] were measured at the beginning and end of each analytical session and after every 50 analyses. Back-scattered electron images were obtained in the COMPO Image mode at a beam current of 20 nA.

## PETROGRAPHIC AND MINERALOGICAL CHARACTERISTICS OF ROCKS

### *Petrography*

Macroscopically, the peridotites are yellowish green (serpentinized lherzolites) or light red (serpentinized dunites) fine-grained polymineralic rocks (Figs. 2a, 2d). All the rocks are almost completely serpentinized (lherzolites) and silicified (dunites and some lherzolites) and show a heterogeneous structure and a reticulate texture. The degree of lherzolite serpentinization is very high and may reach 80–100%. One of the serpentinized lherzolite samples (DR37-14) shows characteristic features of stress-induced solid-state plastic deformations. Serpentine is represented by reticulate chrysotile. The altered dunites show clear indications of specific low-temperature processes resulting in their silicification and replacement of all silicate phases by quartz and amorphous silica [8]. Relicts of primary clinopyroxene, orthopyroxene, and chrome spinel were observed in the rocks.

### *Clinopyroxene*

Clinopyroxene grains in the serpentinized lherzolites are up to 0.1 mm in size (occasionally up to 0.4 mm) and account for 15% of the rocks (Fig. 2b). They are unevenly distributed in the samples and most abundant around large orthopyroxene grains. Some clinopyroxene grains are replaced by homoaxial calcic amphibole pseudomorphs. The pseudomorphic character of replacement is gradually obliterated by super-

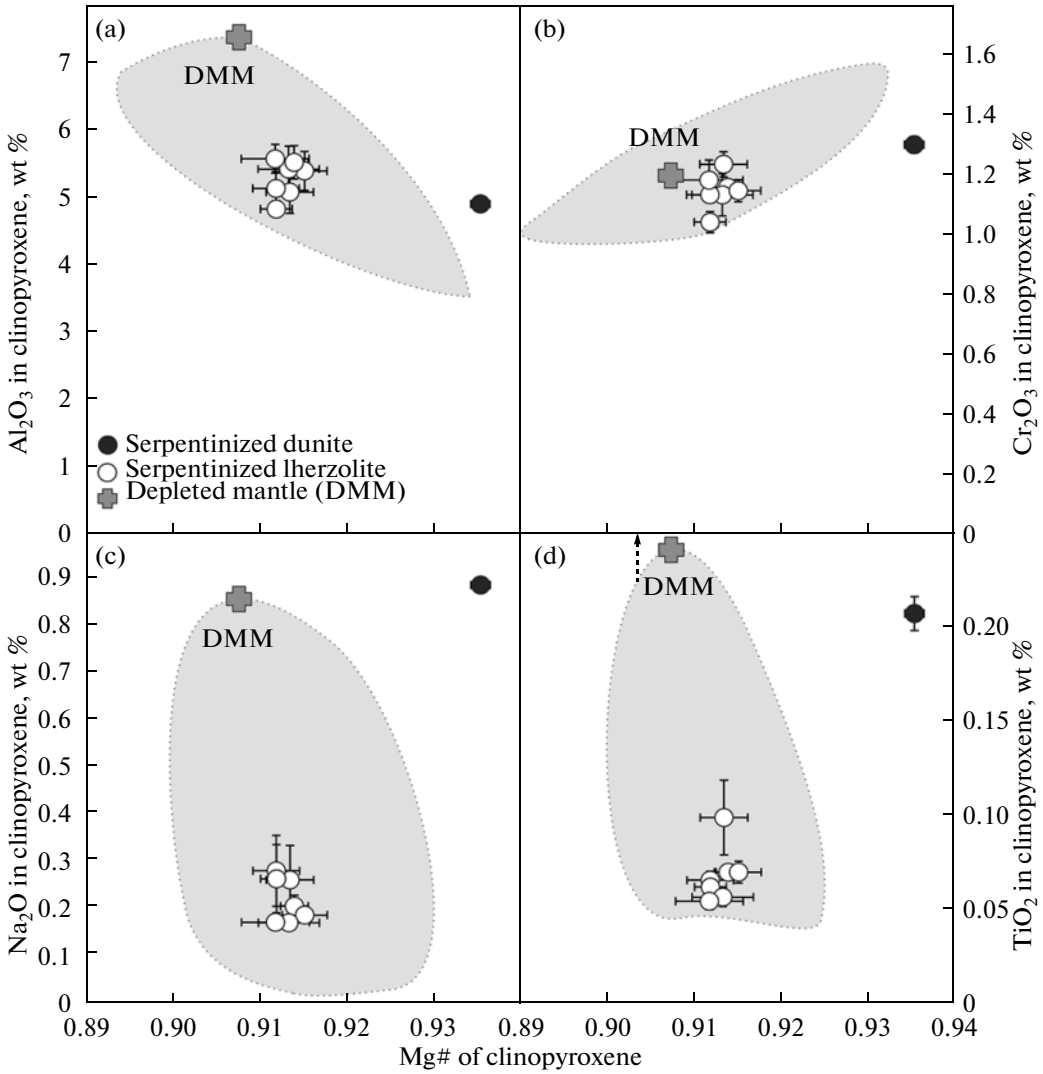


**Fig. 3.** Covariations of Mg# = Mg/(Mg + Fe) with the contents (wt %) of (a) $Al_2O_3$, (b) $Cr_2O_3$, (c) $Na_2O$, and (d) $TiO_2$ in clinopyroxene from the peridotites of the Stalemate Ridge. The shaded fields are the mean compositions of typical abyssal peridotites after [19, 21], and the gray cross is the composition of the depleted mantle [15].

imposed deformations. This results in the formation of thin plates of calcic amphibole. Thin clinopyroxene lamellae up to 1 μm thick exsolved from solid solution also occur in orthopyroxene. Clinopyroxene is very rare in the serpentinized dunites and was never observed in thin sections. The pyroxenes that were analyzed are separate homogeneous fragments of crystals without any evidence for solid solution decomposition from the 0.25–1.0 mm fraction of the crushed rock.

Clinopyroxene from the lherzolites shows a moderately magnesian (Mg# = 100Mg/(Mg + Fe) = 91.7–92.4) and chromian (Cr# = Cr/(Cr + Al) = 0.12–0.16) composition corresponding to the range of clinopyroxene compositions from moderately depleted MOR peridotites ($Na_2O$ = 0.19–0.41 wt %, $TiO_2$ = 0.06–0.15 wt %, $Al_2O_3$ = 3.59–5.48 wt %, $Cr_2O_3$ = 0.82–1.18 wt %, and NiO = 0.06–0.09 wt %) (Table 1, Fig. 3) [10, 11]. Clinopyroxene from silicified dunite sample DR37-3 is sharply different in composition from lherzolitic clinopyroxene in higher Mg# (93.7); higher contents of $Na_2O$ (0.85 wt %), $TiO_2$ (0.23 wt %), and $Cr_2O_3$ (1.32 wt %); and lower $Al_2O_3$ (4.65 wt %) and NiO (0.06 wt %) (Fig. 3, Table 1). Clinopyroxene from lherzolite sample DR37-6 (Fig. 3) shows an intermediate composition between clinopyroxenes from the lherzolites and dunites (Mg# = 92.4, $Na_2O$ = 0.21 wt %, $TiO_2$ = 0.14 wt %, $Cr_2O_3$ = 0.82 wt %, and NiO = 0.08 wt %). Figure 4 shows the mean compositions of basalts from the East Pacific Rise [12, 13] and mean compositions of diabases from ODP Hole 504B [14]. Perhaps, the systematic enrichment of clinopyroxenes from the dunite and lherzolite (mainly, DR-37-6) in Na and Ti is related to the interaction of peridotitic (lherzolitic) material with basaltic melt. Cli-

**Table 1.** Mean compositions of clinopyroxene from the serpentinized dunite (sample DR37-3) and lherzolites (samples DR37-5, DR37-6, DR37-7, DR37-9, DR37-10, DR37-11, DR37-12, DR37-13, DR37-14, and DR37-15) of the Stalemate Ridge; *n* is the number of analyses; σ is standard deviation; Cr# = Cr/(Cr + Al); and Mg# = Mg/(Mg + Fe)

| Component | DR37-3 | DR37-6 | DR37-9 | DR37-10 | DR37-11 | DR37-12 | DR37-13 | DR37-14 | DR37-15 |
|---|---|---|---|---|---|---|---|---|---|
| | Number of analyses | | | | | | | | |
| | 4 | 6 | 4 | 2 | 3 | 11 | 13 | 3 | 3 |
| $SiO_2$ | 51.61 | 53.62 | 51.41 | 51.41 | 51.65 | 51.33 | 51.30 | 51.69 | 52.02 |
| $TiO_2$ | 0.21 | 0.14 | 0.07 | 0.07 | 0.07 | 0.06 | 0.05 | 0.10 | 0.06 |
| $Al_2O_3$ | 4.90 | 3.59 | 5.39 | 5.52 | 5.13 | 5.41 | 5.57 | 5.07 | 4.82 |
| $Cr_2O_3$ | 1.32 | 0.82 | 1.16 | 1.18 | 1.15 | 1.15 | 1.20 | 1.25 | 1.06 |
| FeO | 1.84 | 2.49 | 2.87 | 2.95 | 2.94 | 2.88 | 2.96 | 3.03 | 3.01 |
| MnO | 0.02 | 0.08 | 0.08 | 0.08 | 0.07 | 0.08 | 0.08 | 0.07 | 0.07 |
| MgO | 14.99 | 16.90 | 17.36 | 17.57 | 17.08 | 17.03 | 17.12 | 17.95 | 17.49 |
| CaO | 23.33 | 23.31 | 21.00 | 20.54 | 21.16 | 21.43 | 21.16 | 20.10 | 20.94 |
| $Na_2O$ | 0.89 | 0.35 | 0.19 | 0.21 | 0.28 | 0.17 | 0.17 | 0.26 | 0.27 |
| NiO | 0.06 | 0.08 | 0.10 | 0.10 | 0.07 | 0.10 | 0.11 | 0.11 | 0.11 |
| Total | 99.17 | 101.38 | 99.64 | 99.61 | 99.61 | 99.66 | 99.72 | 99.64 | 99.85 |
| Mg# | 0.94 | 0.92 | 0.92 | 0.91 | 0.91 | 0.91 | 0.91 | 0.91 | 0.91 |
| Cr# | 0.15 | 0.13 | 0.13 | 0.13 | 0.13 | 0.12 | 0.13 | 0.14 | 0.13 |
| Standard deviation (σ) | | | | | | | | | |
| $SiO_2$ | 0.06 | 0.64 | 0.29 | 0.06 | 0.26 | 0.27 | 0.20 | 0.18 | 0.27 |
| $TiO_2$ | 0.01 | 0.04 | 0.01 | 0.00 | 0.00 | 0.00 | 0.00 | 0.02 | 0.01 |
| $Al_2O_3$ | 0.04 | 0.67 | 0.29 | 0.25 | 0.25 | 0.34 | 0.21 | 0.32 | 0.12 |
| $Cr_2O_3$ | 0.03 | 0.19 | 0.04 | 0.01 | 0.03 | 0.07 | 0.07 | 0.04 | 0.04 |
| FeO | 0.04 | 0.24 | 0.28 | 0.23 | 0.18 | 0.16 | 0.27 | 0.19 | 0.13 |
| MnO | 0.01 | 0.02 | 0.02 | 0.01 | 0.02 | 0.02 | 0.01 | 0.01 | 0.01 |
| MgO | 0.07 | 0.33 | 1.12 | 0.99 | 0.65 | 0.50 | 0.90 | 0.53 | 0.39 |
| CaO | 0.04 | 0.67 | 1.38 | 1.38 | 0.60 | 0.71 | 1.29 | 0.83 | 0.66 |
| $Na_2O$ | 0.01 | 0.03 | 0.02 | 0.02 | 0.08 | 0.01 | 0.01 | 0.07 | 0.07 |
| NiO | 0.03 | 0.04 | 0.03 | 0.05 | 0.02 | 0.02 | 0.03 | 0.03 | 0.01 |
| Total | 0.11 | 0.34 | 0.18 | 0.19 | 0.13 | 0.15 | 0.20 | 0.09 | 0.13 |
| Mg# | 0.00 | 0.63 | 0.00 | 0.00 | 0.00 | 0.00 | 0.00 | 0.00 | 0.00 |
| Cr# | 0.16 | 0.01 | 0.59 | 0.40 | 0.43 | 0.44 | 0.39 | 0.64 | 0.11 |

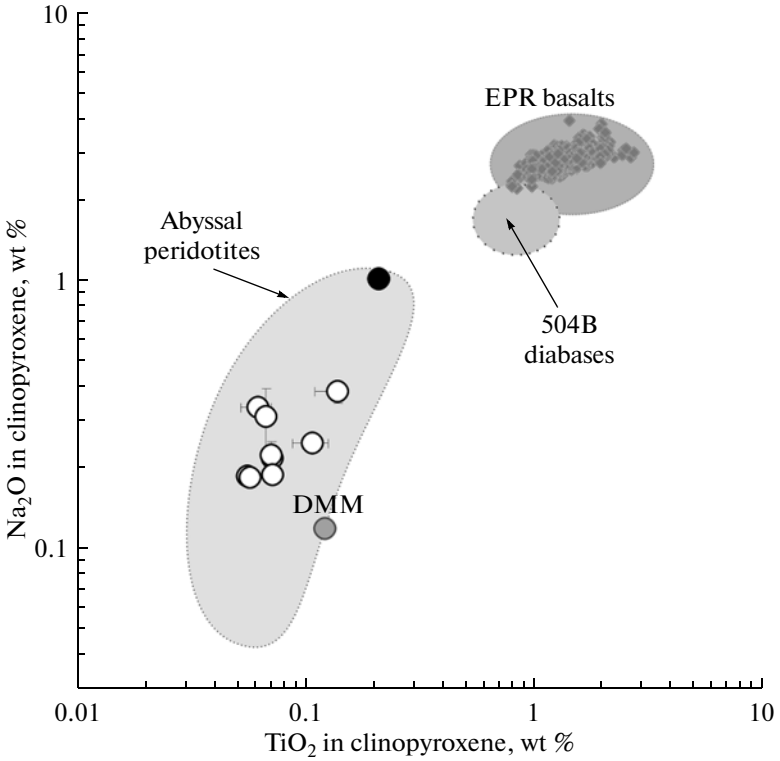


**Fig. 4.** Systematics of Na and Ti variations in clinopyroxene from the peridotites of the Stalemate Fracture Zone. The compositions of clinopyroxene from serpentinized lherzolite and dunite are shown by unfilled and filled circles, respectively. The mean composition of basalts from the East Pacific Rise is taken from [12, 13], the mean composition of diabases from Hole 504B is after [14], the field of abyssal peridotites is outlined using the data of [16], and the gray circle is the composition of the depleted mantle [15].

nopyroxene lamellae in orthopyroxene are narrow micrometer-sized stringers (Figs. 2b, 2c), which could not be analyzed.

### *Orthopyroxene*

The serpentinized lherzolites contain from 10 to 20% orthopyroxene. Orthopyroxene grains are pseudomorphed by bastite serpentine. Unaltered relicts occur as small anhedral grains usually no more than 0.1 mm in size, occasionally up to 0.4 mm. The margins of large orthopyroxene phenocrysts are fractured, and numerous small grains of orthopyroxene occur in the enclosing rock matrix. Orthopyroxene contains platy ingrowths of clinopyroxene formed by the decomposition of solid solution (Fig. 2c). Orthopyroxene lamellae occur in turn in large clinopyroxene grains. Orthopyroxene was not detected in the altered dunites.

The compositions of orthopyroxene fall within a narrow interval (Fig. 5, Table 2; Mg# = 90.3–90.9, $TiO_2$ = 0.02–0.05 wt %, $Na_2O$ = 0.01–0.025 wt %, $Al_2O_3$ = 3.86–4.85 wt %, $Cr_2O_3$ = 0.61–0.81 wt %, and NiO = 0.12–0.17 wt %). With respect to Cr and Al contents, orthopyroxene from the lherzolites of the Stalemate Ridge corresponds to orthopyroxene from the moderately depleted peridotites of the Mid-Atlantic Ridge (Fig. 6) and is different from orthopyroxene from the peridotites of the East Pacific Rise in higher Al content ($Al_2O_3$ = 2.1–2.9 wt %) [12].

### *Chrome Spinel*

Spinel of two morphological types occurs in the lherzolites. One type includes large irregular grains from 0.4 to 0.6 mm in size, and the other is small crystals 0.05–0.1 mm in size forming aggregates around clinopyroxene grains (Fig. 2a). The altered dunites contain irregular spinel grains from 0.1 to 0.25 mm in size embedded in a silicified matrix (Fig. 2d).

Spinel from the peridotites of the Stalemate Fracture Zone shows considerable compositional variations (Figs. 7, 8; Table 3). The lherzolites contain moderately chromian (Cr# = 0.27–0.33) and moderately magnesian (Mg# = 0.65–0.69) spinel with low Ti ($TiO_2$ = 0.04–0.09 wt %) and $Fe^{3+}$ ($Fe^{3+}$# = 0.021–0.029). Spinel from the altered dunites is more chromian (Cr# = 0.39–0.43), titanian ($TiO_2$ = 0.19–0.28 wt %), and oxidized ($Fe^{3+}$# = 0.027–0.043). The composition of spinel from sample DR37-6 is intermediate between the lherzolitic and dunitic spinels (Cr# = 0.33, $Fe^{3+}$# = 0.022, and $TiO_2$ = 0.09 wt %). The compositions of spinel and clinopyroxene are strongly correlated in the

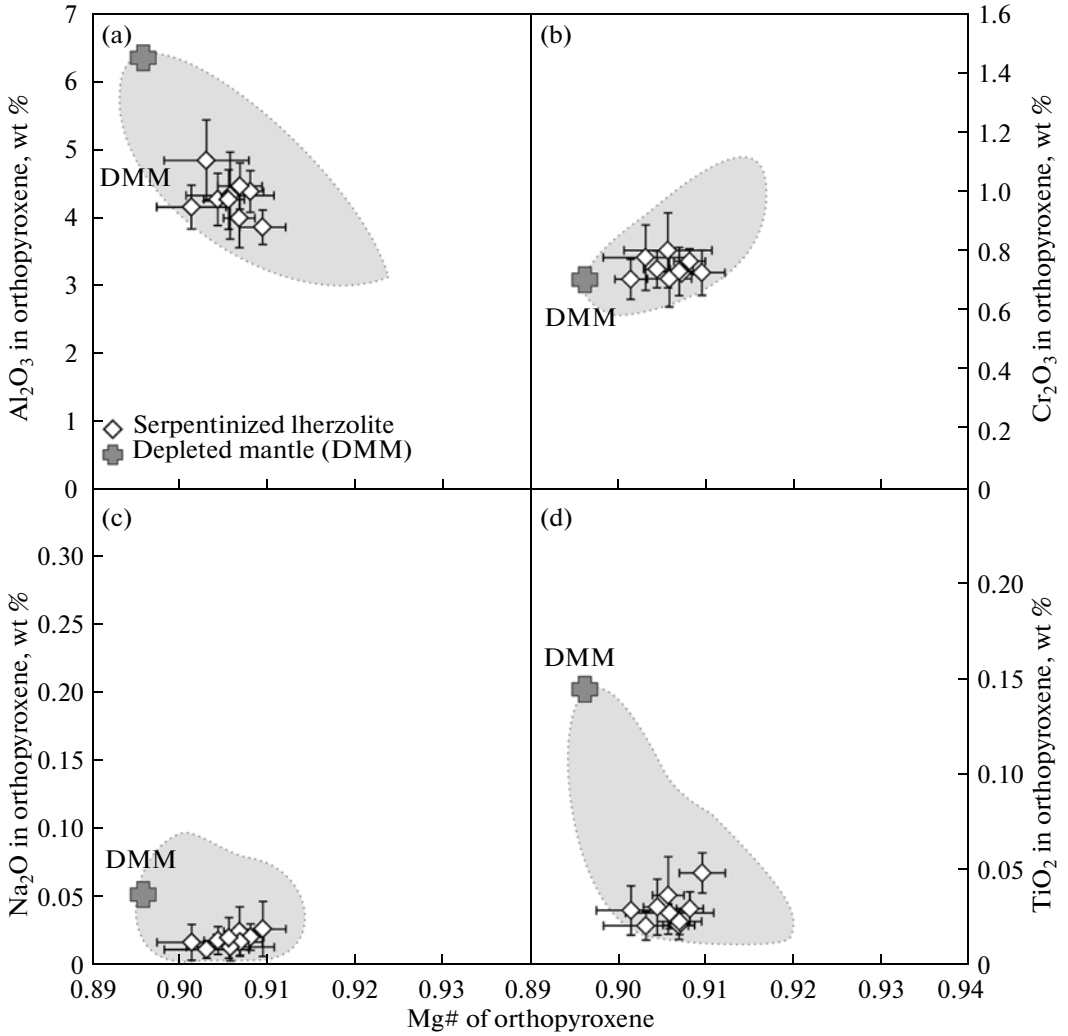


**Fig. 5.** Covariations of Mg# = Mg/(Mg + Fe) with the contents (wt %) of (a) $Al_2O_3$, (b) $Cr_2O_3$, (c) $Na_2O$, and (d) $TiO_2$ in orthopyroxenes from the peridotites of the Stalemate Ridge. Gray fields show the mean composition of typical abyssal peridotites [19, 21], and the gray cross is the composition of the depleted mantle [15].

rocks (Fig. 8). An increase in Cr# and $TiO_2$ content from the lherzolites to the dunites is accompanied by an increase in $TiO_2$ and $Na_2O$ in clinopyroxene (Fig. 8).

## DISCUSSION

### *Genesis of Lherzolites*

The composition of minerals from the altered lherzolites is consistent with the compositional fields of phases from the residual peridotites of MOR [17], which suggests that the lherzolites can be interpreted as products of partial melting of the upper mantle beneath the Kula–Pacific Ridge. In order to estimate the conditions of mantle melting, geochemical modeling was performed on the basis of spinel (Cr# and Ti) and clinopyroxene (Ti) compositions from the lherzolites. We used the models of critical and nonmodal melting of an initial four-phase assemblage [18], which are based on the calculated data on the congruent melting of undepleted MORB-type lherzolite. The chemical composition of the model mantle source was taken to correspond to the depleted mantle (DMM), and its mineral composition and melting reaction were adopted from Brunelli et al. [19]. Currently, the mineral/melt partitioning of major elements is not yet fully understood. Therefore, modeling reported in this paper (Figs. 8b, 8d) was performed for different mineral/melt partition coefficients accounting for possible variations in the temperature and pressure of mantle melting. The partition coefficients of titanium between clinopyroxene and melt ($Kd^{Ti}_{Cpx}$ = 0.1–0.35) and spinel and melt ($Kd^{Ti}_{Sp}$ = 0.048–0.15) were taken after [16, 20]. Hellebrand et al. [21] presented empirical dependence between the degree of mantle melting and the compositional parameters of coexisting spinel and clinopyroxene in the residue: the contents of heavy rare earth elements (Dy, Er,

**Table 2.** Mean compositions of orthopyroxene from the serpentinized lherzolites of the Stalemate Ridge; Cr# = Cr/(Cr + Al) and Mg# = Mg/(Mg + Fe)

| Component | DR37-5 | DR3-6 | DR37-9 | DR37-10 | DR37-11 | DR37-12 | DR37-13 | DR37-14 | DR37-15 |
|---|---|---|---|---|---|---|---|---|---|
| | Number of analyses | | | | | | | | |
| | 12 | 29 | 14 | 19 | 31 | 28 | 41 | 42 | 26 |
| $SiO_2$ | 55.26 | 55.96 | 56.25 | 55.21 | 55.32 | 55.26 | 55.28 | 55.41 | 55.53 |
| $TiO_2$ | 0.02 | 0.05 | 0.02 | 0.03 | 0.03 | 0.02 | 0.03 | 0.04 | 0.03 |
| $Al_2O_3$ | 4.85 | 3.86 | 4.00 | 4.39 | 4.27 | 4.47 | 4.33 | 4.27 | 4.16 |
| $Cr_2O_3$ | 0.78 | 0.73 | 0.61 | 0.77 | 0.74 | 0.73 | 0.71 | 0.81 | 0.71 |
| FeO | 6.30 | 5.89 | 6.08 | 5.95 | 6.23 | 6.02 | 6.14 | 6.10 | 6.36 |
| MnO | 0.13 | 0.12 | 0.12 | 0.12 | 0.12 | 0.12 | 0.12 | 0.13 | 0.13 |
| MgO | 32.93 | 33.20 | 33.19 | 32.99 | 33.06 | 32.89 | 33.17 | 32.89 | 32.52 |
| CaO | 1.01 | 1.30 | 1.10 | 1.44 | 1.23 | 1.41 | 1.15 | 1.30 | 1.27 |
| $Na_2O$ | 0.01 | 0.03 | 0.02 | 0.02 | 0.02 | 0.02 | 0.01 | 0.02 | 0.02 |
| NiO | 0.17 | 0.17 | 0.12 | 0.16 | 0.16 | 0.16 | 0.15 | 0.15 | 0.14 |
| Total | 101.46 | 101.31 | 101.37 | 101.09 | 101.19 | 101.13 | 101.09 | 101.13 | 100.87 |
| Mg# | 0.90 | 0.91 | 0.91 | 0.91 | 0.90 | 0.91 | 0.91 | 0.91 | 0.90 |
| Cr# | 0.10 | 0.11 | 0.07 | 0.11 | 0.10 | 0.13 | 0.10 | 0.11 | 0.11 |
| Standard deviation | | | | | | | | | |
| $SiO_2$ | 0.35 | 0.30 | 0.84 | 0.33 | 0.35 | 0.41 | 0.43 | 0.51 | 0.28 |
| $TiO_2$ | 0.01 | 0.01 | 0.01 | 0.01 | 0.01 | 0.01 | 0.01 | 0.02 | 0.01 |
| $Al_2O_3$ | 0.59 | 0.25 | 0.43 | 0.31 | 0.39 | 0.34 | 0.64 | 0.44 | 0.32 |
| $Cr_2O_3$ | 0.11 | 0.08 | 0.04 | 0.06 | 0.08 | 0.09 | 0.13 | 0.07 | 0.09 |
| FeO | 0.26 | 0.23 | 0.24 | 0.14 | 0.11 | 0.18 | 0.24 | 0.15 | 0.33 |
| MnO | 0.04 | 0.03 | 0.03 | 0.02 | 0.02 | 0.03 | 0.03 | 0.03 | 0.04 |
| MgO | 0.57 | 0.75 | 1.43 | 0.45 | 0.40 | 0.50 | 0.78 | 0.54 | 0.54 |
| CaO | 0.42 | 0.66 | 0.46 | 0.39 | 0.37 | 0.54 | 0.39 | 0.54 | 0.61 |
| $Na_2O$ | 0.01 | 0.02 | 0.02 | 0.01 | 0.01 | 0.01 | 0.01 | 0.01 | 0.01 |
| NiO | 0.06 | 0.05 | 0.04 | 0.05 | 0.04 | 0.05 | 0.04 | 0.05 | 0.03 |
| Total | 0.41 | 0.24 | 0.36 | 0.28 | 0.25 | 0.31 | 0.40 | 0.59 | 0.49 |
| Mg# | 0.00 | 0.00 | 0.00 | 0.00 | 0.00 | 0.00 | 0.01 | 0.00 | 0.00 |
| Cr# | 0.01 | 0.01 | 4.87 | 0.00 | 0.01 | 0.17 | 0.01 | 1.17 | 1.01 |

**Table 3.** Mean compositions of spinel from the serpentinized dunites (samples DR37-1, DR37-2, DR37-3, and DR37-4) and lherzolites (samples DR37-5, DR37-6, DR37-9, DR37-10, DR37-11, DR37-12, DR37-13, DR37-14, and DR37-15) of the Stalemate Ridge; Cr# = Cr/(Cr + Al); and Mg# = Mg/(Mg + Fe)

| Component | DR37-1 | DR37-2 | DR37-3 | DR37-4 | DR37-5 | DR37-6 | DR37-9 | DR37-10 | DR37-11 | DR37-12 | DR37-13 | DR37-14 | DR37-15 |
|---|---|---|---|---|---|---|---|---|---|---|---|---|---|
| | Number of analyses | | | | | | | | | | | | |
| | 14 | 16 | 18 | 10 | 11 | 10 | 4 | 9 | 12 | 14 | 10 | 13 | 10 |
| $SiO_2$ | 0.011 | 0.001 | 0.018 | 0.010 | 0.004 | 0.001 | 0.001 | 0.003 | 0.003 | 0.003 | 0.004 | 0.005 | 0.006 |
| $TiO_2$ | 0.257 | 0.282 | 0.209 | 0.235 | 0.043 | 0.090 | 0.045 | 0.049 | 0.042 | 0.043 | 0.043 | 0.050 | 0.049 |
| $Al_2O_3$ | 34.305 | 30.894 | 34.416 | 34.220 | 42.768 | 38.920 | 42.475 | 43.029 | 43.143 | 43.601 | 44.094 | 42.203 | 41.009 |
| $Cr_2O_3$ | 32.778 | 34.274 | 32.364 | 32.601 | 24.275 | 28.684 | 24.885 | 24.207 | 23.744 | 23.801 | 23.269 | 25.213 | 25.735 |
| FeO | 15.510 | 19.141 | 15.837 | 15.884 | 14.675 | 14.869 | 14.035 | 14.014 | 14.969 | 14.072 | 14.085 | 14.339 | 15.776 |
| MnO | 0.141 | 0.165 | 0.133 | 0.136 | 0.120 | 0.132 | 0.118 | 0.123 | 0.119 | 0.118 | 0.111 | 0.122 | 0.128 |
| MgO | 15.649 | 13.527 | 15.197 | 15.632 | 16.805 | 16.074 | 16.883 | 17.053 | 16.559 | 17.194 | 17.022 | 16.906 | 16.108 |
| NiO | 0.248 | 0.195 | 0.247 | 0.254 | 0.327 | 0.261 | 0.305 | 0.296 | 0.330 | 0.338 | 0.343 | 0.332 | 0.284 |
| Total | 98.898 | 98.479 | 98.422 | 98.971 | 99.018 | 99.031 | 98.747 | 98.774 | 98.909 | 99.170 | 98.971 | 99.169 | 99.095 |
| Mg# | 0.642 | 0.558 | 0.631 | 0.637 | 0.671 | 0.658 | 0.682 | 0.684 | 0.663 | 0.685 | 0.683 | 0.678 | 0.645 |
| Cr# | 0.391 | 0.427 | 0.387 | 0.390 | 0.276 | 0.331 | 0.282 | 0.274 | 0.270 | 0.268 | 0.262 | 0.286 | 0.296 |
| Standard deviation | | | | | | | | | | | | | |
| $SiO_2$ | 0.009 | 0.003 | 0.026 | 0.009 | 0.004 | 0.003 | 0.002 | 0.006 | 0.004 | 0.004 | 0.007 | 0.006 | 0.007 |
| $TiO_2$ | 0.017 | 0.035 | 0.013 | 0.015 | 0.005 | 0.011 | 0.008 | 0.008 | 0.007 | 0.007 | 0.007 | 0.006 | 0.014 |
| $Al_2O_3$ | 0.846 | 1.089 | 0.397 | 0.197 | 1.200 | 0.768 | 0.634 | 0.666 | 1.284 | 0.608 | 1.135 | 0.740 | 1.035 |
| $Cr_2O_3$ | 0.710 | 0.475 | 0.525 | 0.412 | 1.001 | 0.953 | 0.486 | 0.838 | 1.209 | 0.788 | 1.275 | 0.755 | 1.191 |
| FeO | 1.395 | 1.426 | 0.231 | 0.160 | 1.216 | 0.358 | 0.527 | 0.293 | 0.675 | 0.395 | 0.469 | 0.305 | 0.549 |
| MnO | 0.026 | 0.024 | 0.011 | 0.016 | 0.021 | 0.024 | 0.016 | 0.021 | 0.019 | 0.021 | 0.016 | 0.012 | 0.025 |
| MgO | 0.996 | 0.677 | 0.903 | 0.755 | 0.776 | 0.435 | 0.330 | 0.125 | 0.457 | 0.441 | 0.397 | 0.192 | 0.365 |
| NiO | 0.027 | 0.032 | 0.024 | 0.029 | 0.041 | 0.030 | 0.054 | 0.032 | 0.049 | 0.038 | 0.030 | 0.018 | 0.031 |
| Total | 0.318 | 0.392 | 0.686 | 0.405 | 0.195 | 0.315 | 0.166 | 0.114 | 0.243 | 0.368 | 0.419 | 0.118 | 0.223 |
| Mg# | 0.035 | 0.026 | 0.014 | 0.011 | 0.029 | 0.009 | 0.012 | 0.006 | 0.016 | 0.009 | 0.007 | 0.007 | 0.013 |
| Cr# | 0.010 | 0.010 | 0.006 | 0.003 | 0.014 | 0.012 | 0.007 | 0.010 | 0.016 | 0.009 | 0.015 | 0.010 | 0.015 |

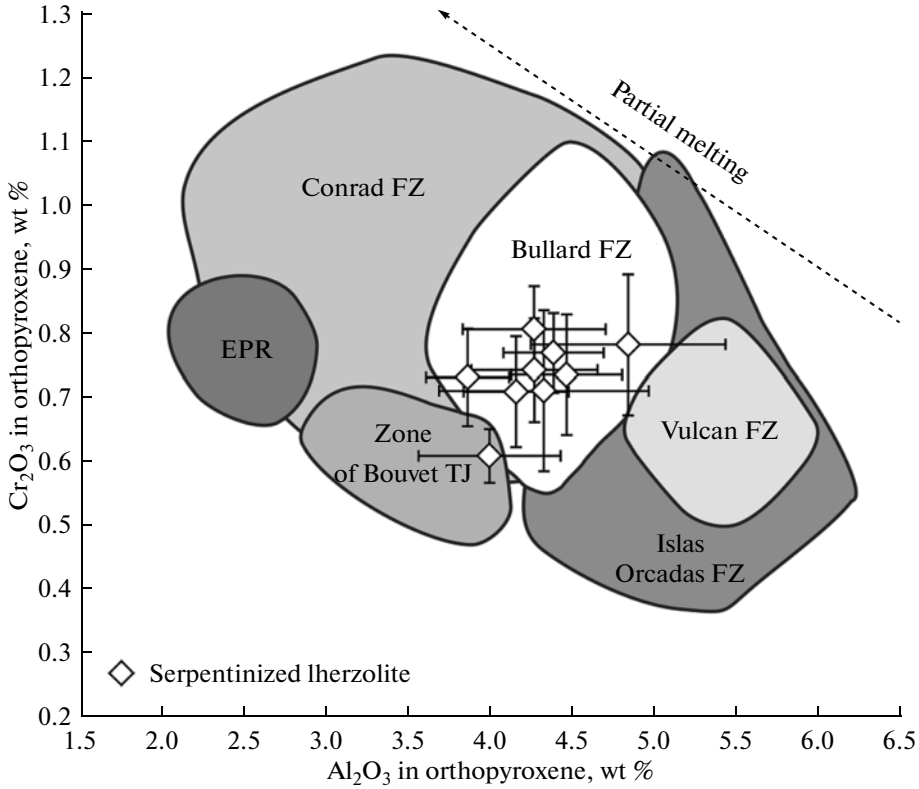


**Fig. 6.** Systematics of Al and Cr variations in orthopyroxene from the peridotites of the Stalemate Fracture Zone. The diagram shows the mean compositions of orthopyroxene from the serpentinized lherzolites of the Stalemate Fracture Zone and some characteristic fields after [23].

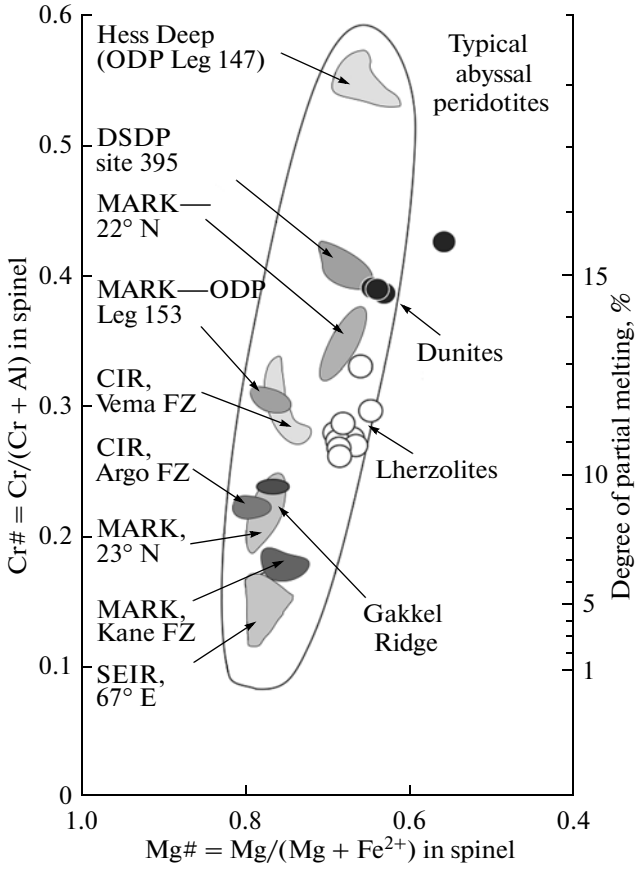


and Yb) in clinopyroxene and Cr# of coexisting spinel. In such a way, an empirical relation was obtained between the Cr# of spinel in the mantle residue and the degree of fractional melting. The composition of the mantle source in the established dependence was accepted as the composition of the depleted mantle. The degree of melting of the mantle source of the lherzolites of the Stalemate Fracture Zone was therefore calculated using the equation [21]

$$F = 10 * \ln(\text{Cr\#Sp}) + 24,$$

where $F$ is the degree of melting, and Cr#Sp is Cr/(Cr + Al) in spinel.

The results of our modeling (Figs. 8b, 8d) indicate that the observed spinel and clinopyroxene compositions from the lherzolites can be explained by 10–12% near-fractional melting of a depleted mantle source (DMM) at $Kd^{Ti}_{Cpx} = 0.15$ and $Kd^{Ti}_{Sp} = 0.1$. With respect to the estimated parameters of formation, the lherzo-

**Fig. 7.** Covariations of Cr# = Cr/(Al + Cr) and Mg# = Mg/(Mg + Fe) in spinel from the peridotites of the Stalemate Fracture Zone. The compositional fields of peridotites from various MOR segments, including the Southeastern Indian Ridge (SEIR), Central Indian Ridge (CIR), and region of the Kane Fracture Zone of the Mid-Atlantic Ridge (MARK) are shown after [19].

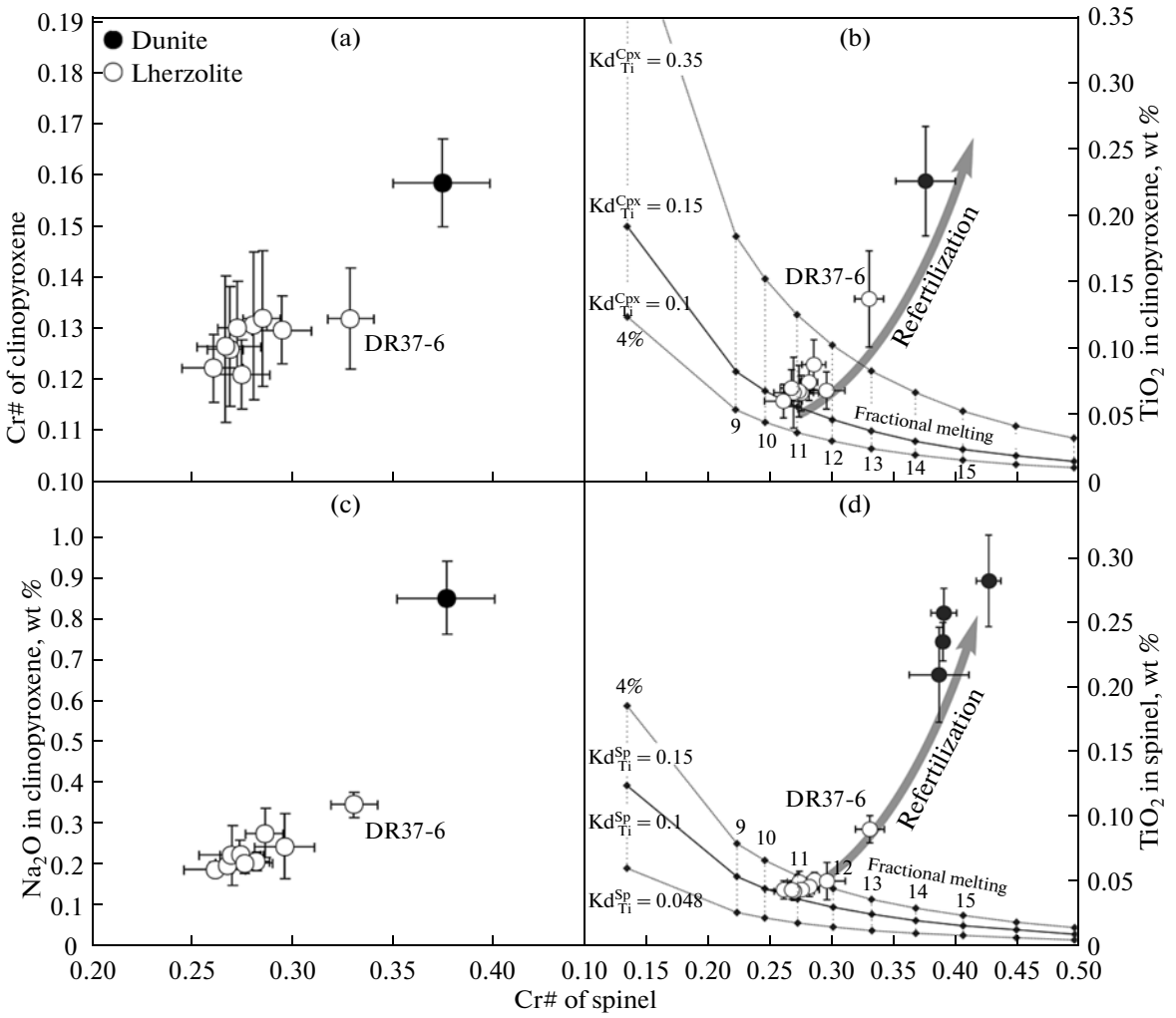


**Fig. 8.** Covariations of Cr# = Cr/(Al + Cr) values in spinel with (a) Cr# of clinopyroxene, (b) $TiO_2$ in clinopyroxene, (c) $Na_2O$ in clinopyroxene, and (d) $TiO_2$ in spinel for the peridotites of the Stalemate Ridge. Rock symbols are the same as in Fig. 3. Also shown in Figs. 8b and 8d are the results of geochemical modeling for the compositions of spinel (Cr# and Ti) and clinopyroxene (Ti) from the lherzolites described here. Thin lines are partial melting trends calculated using partition coefficients of $Kd_{Ti}^{Cpx} = 0.01$ and $Kd_{Ti}^{Sp} = 0.048$ [20] or $Kd_{Ti}^{Cpx} = 0.35$ and $Kd_{Ti}^{Sp} = 0.15$ [16]. The bold line is the trend of fractional melting of a material corresponding to the serpentinized lherzolites of the Stalemate Fracture Zone.

lites of the Stalemate Ridge are similar to the residual peridotites of Mid-Atlantic Ridge, for instance, from the Vema Fracture Zone of the MAR (Fig. 7). The peridotites of the East Pacific Rise were produced by significantly higher degrees of mantle melting reaching ~18% (Fig. 7).

### *Genesis of Dunites*

The compositions of primary minerals from the lherzolites and dunites straddle common trends (Fig. 8), which implies a close genetic relation between these rocks. However, the positive correlations between Cr# and Ti in spinel and between Cr# in spinel and Na and Ti in clinopyroxene cannot be explained by the progressive depletion of the mantle source from lherzolite to dunite owing to partial melting. Therefore, the compositions of spinel and pyroxene in the dunites and lherzolite sample DR37-6 strongly deviating from the expected partial melting trends should be interpreted in a different way. A viable model for the formation of dunites in the Stalemate Fracture Zone is low-pressure interaction of lherzolites with Na- and Ti-rich magmatic melts. This process could result in pyroxene dissolution in the lherzolite, development of reaction infiltration instability (refertilization), and formation of a system of dunite channels marking melt transport paths to the surface (Fig. 8) [3]. Thus, the dunites are considered as igneous rocks of a reaction origin affected by fluid–magma refertilization owing to melt infiltration through them. The lherzolite–dunite association dredged from the Stalemate Ridge can be interpreted as

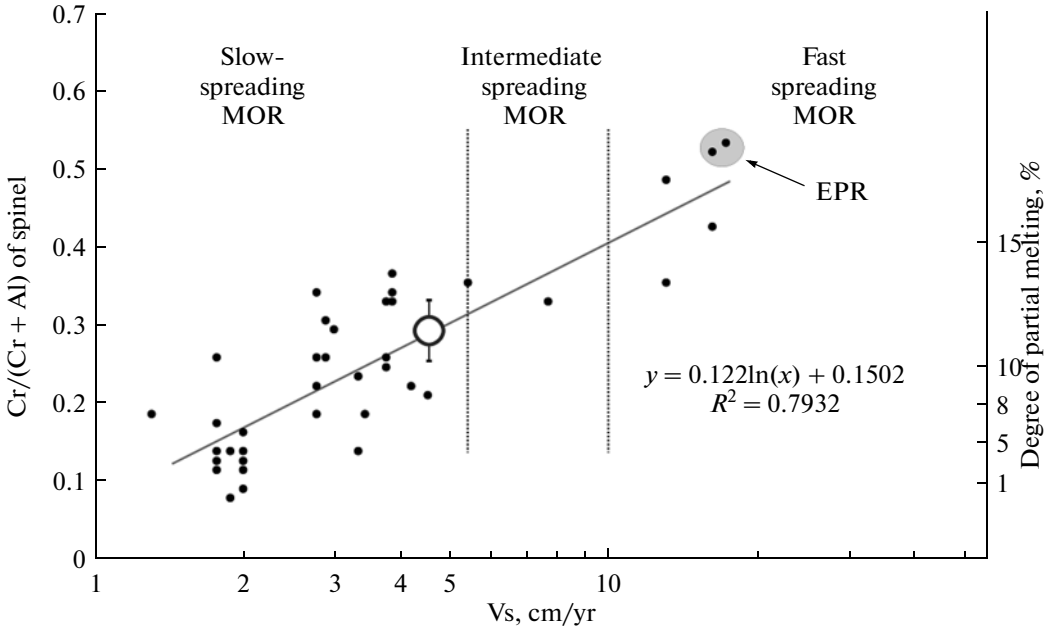


**Fig. 9.** Correlation of the mean Cr# value of spinel and full spreading rate (Vs). The unfilled circle shows the mean composition of spinel from the serpentinized lherzolites of the Stalemate Fracture Zone. The Cr# values and the degrees of partial melting are after Bazylev and Silantyev [22].

a fragment of the oceanic lithospheric mantle consisting of residual lherzolites and dunite channels.

### *Geochemical Constraints for the Spreading Rate of the Kula–Pacific Paleoridge*

Bazylev and Silantyev [22] estimated variations in Cr# of spinel and degree of partial melting as functions of the spreading rate. In slow-spreading ridge environments (full spreading rate of up to 5.5 cm/yr), the Cr# value of primary spinels in mantle peridotites ranges from 0.11 to 0.45, whereas in fast-spreading ridges (with a full spreading rate higher than 10 cm/yr), this parameter is 0.35–0.55. The spinel lherzolites of the Stalemate Fracture Zone contain moderately chromian spinel (Cr# = 0.26–0.33) corresponding to the compositions of spinel from the peridotites of slow-spreading ridge (Fig. 9). Using the correlation of Bazylev and Silantyev [22], the full spreading rate during the formation of the Stalemate Ridge peridotites can be estimated as 4–5 cm/yr. This estimate is well consistent with paleomagnetic observations [3], which were used to estimate the full spreading rate of the ancient Kula–Pacific Ridge as 6.5 cm/yr (approximately 2 cm/yr to the west and 4.5 cm/yr to the east). The spreading rate of the Kula–Pacific paleoridge estimated on the basis of geochemical and paleomagnetic data is much lower than that of the fast-spreading ridges of the modern Pacific Ocean [22]. The compositions of peridotites obtained in this study and paleomagnetic data [3] provide compelling evidence for the existence of slow-spreading ridges in the Pacific Ocean basin in the past. This suggests that the geodynamics of the rift zones of the Pacific Ocean has changed considerably since 43 Ma (age of cessation of Kula–Pacific spreading).

## CONCLUSIONS

The association of peridotites dredged from the Stalemate Ridge in 2009 during cruise SO201-1b KALMAR of the R/V *Sonne* includes serpentinized lherzolites and serpentinized silicified dunites. The analysis of coexisting relicts of primary mantle minerals in the rocks allowed us to elucidate the genesis of these rocks and estimate the spreading rate of the Kula–Pacific paleoridge. The observed compositional variations of coexisting clinopyroxene and spinel could be related to a two-stage process of formation of these rocks. During the first stage, 10–12% near-fractional melting of a depleted mantle source of the DMM type produced depleted lherzolites. During the second stage, the interaction of the residual lherzolites with Na- and Ti-rich melts resulted in the formation of reaction dunites. Thus, the protolith of the serpentinized lherzolites and dunites of the Stalemate Fracture Zone was represented by fragments of shallow oceanic mantle partly modified by percolating deep melts. The results of our investigation suggest a relation of the rocks of the lherzolite–dunite association of the Stalemate Fracture Zone with the ancient mantle material of the Cretaceous–Paleogene lithosphere of the Kula plate. The low Cr# value of spinel from the lherzolites studied here clearly distinguishes these rocks from the peridotites of the East Pacific Rise and indicates the existence of slow-spread-

ing mid-ocean ridges in the Pacific Ocean basin during the Cretaceous–Paleogene.

## ACKNOWLEDGMENTS

The authors are grateful to the research staff of cruise SO201-1b and the crew of the R/V *Sonne* for close and fruitful cooperation, which led to the success of the expedition and collection of material for this study. Special thanks are due to B.A. Bazylev for his assistance and comments to the manuscript. This study was supported by the Russian–German KALMAR Project and the Russian Foundation for Basic Research, project nos. 09-05-00008a and 12-05-00002a; cruise SO201-1b was supported by the German Ministry of Education and Research (BMBF).

## REFERENCES

1. W. C. Pitman and D. E. Hayes, "Seafloor spreading in the Gulf of Alaska," J. Geophys. Res. **73**, 6571–6580 (1968).
2. J. A. Grow and T. Atwater, "Mid-Tertiary tectonic transition in the Aleutian arc," Geol. Soc. Am. Bull. **81**, 4637–4646 (1970).
3. P. Lonsdale, "Paleogene history of the Kula plate: offshore evidence and onshore implications," Geol. Soc. Am. Bull. **100**, 733–754 (1988).
4. D. K. Rea and J. M. Dixon, "Late Cretaceous and Paleogene tectonic evolution of the North Pacific Ocean," Earth Planet. Sci. Lett. **64**, 67–73 (1983).
5. E. Bonatti, "Vertical tectonism in oceanic fracture zones," Earth Planet. Sci. Lett. **37** (3), 369–379 (1978).
6. E. Bonatti, D. Brunelli, W. R. Buck, A. Cipriani, P. Fabretti, V. Ferrante, L. Gasperini, and M. Ligi, "Flexural uplift of a lithospheric slab near the Vema Transform (Central Atlantic): timing and mechanisms," Earth Planet. Sci. Lett. **240** (3–4), 642–655 (2005).
7. F. S. Sonne, *Fahrbericht. Cruise Rept. O201–1*, (KALMAR, 2009), No. 32. www.ifm-geomar.de/fileadmin/ifm-geomar/fuer_alle/institut/publikationen/ifm-geomar_rep32.pdf
8. S. A. Silantyev, A. A. Novoselov, E. A. Krasnova, M. V. Portnyagin, F. Hauff, and R. Werner, "Silicification of peridotites at the Stalemate fracture zone (Northwestern Pacific): reconstruction of the conditions of low-temperature weathering and tectonic interpretation," Petrology **20** (1), 21–39 (2012).
9. E. J. Jarosewich, J. A. Nelen, and J. A. Norberg, "Reference samples for electron microprobe analysis," Geostand. Newslett. **4**, 43–47 (1980).
10. B. A. Bazylev, R. Magakyan, S. A. Silantyev, K. I. Ignatenko, T. V. Romashova, and K. Ksenofontos, "Petrology of the Mamoniya ultrabasic complex, Southwestern Cyprus," Petrologiya **1** (4), 348–378 (1993).
11. T. J. Falloon, D. H. Green, L. V. Danyushevsky, and U. H. Faul, "Peridotite melting at 1.0 and 1.5 GPa: an experimental evaluation of techniques using diamond aggregates and mineral mixes for determination of near-solidus," J. Petrol. **40**, 1343–1375 (1999).
12. *RIDGE, Petrological Data Baseline* (LGEO, Lamont-Doherty Observatory, New York, 1999).
13. W. G. Melson, T. L. Vallier, T. L. Wright, G. Byerly, and J. Nelen, "Chemical diversity of abyssal volcanic glass erupted along Pacific, Atlantic and Indian Ocean seafloor spreading centers," in *The Geophysics of the Pacific Ocean Basin and its Margin*, (Am. Geophys. Union, Washington, 1976), pp. 351–367.
14. J. W. Sparks, "Geochemisty of the lower sheeted dike complex, hole 504B, Leg, 140," Proc. ODP., Sci. Res., **137–140**, 81–97 (1995).
15. R. K. Workman and S. R. Hart, "Major and trace element composition of the depleted MORB mantle (DMM)," Earth Planet. Sci. Lett. **231**, 52–72 (2005).
16. K. T. M. Johnson, H. J. B. Dick, and N. Shimizu, "Melting in the oceanic upper mantle: a ion microprobe study of diopsides in abyssal peridotites," J. Geophys. Res. **95** (B3), 2661–2678 (1990).
17. H. J. B. Dick, R. L. Fisher, and W. B. Bryan, "Mineralogic variability of the uppermost mantle along mid-ocean ridges," Earth Planet. Sci. Lett. **69**, 88–106 (1984).
18. D. M. Shaw, "Trace element fractionation during anatexis," Geochim. Cosmochim. Acta **34**, 237–243 (1970).
19. D. Brunelli, M. Seyler, A. Cipriani, L. Ottolini, and E. Bonatti, "Discontinuous melt extraction and weak refertilization of mantle peridotites at the Vema lithospheric section (Mid-Atlantic ridge)," J. Petrol. **47** (4), 745–771 (2006).
20. D. McKenzie and R. K. O' Nions, "Partial melt distributions from inversion of rare earth element concentrations," J. Petrol. **32**, 1021–1091 (1991).
21. E. Hellebrand, J. E. Snow, and R. Muehe, "Mantle melting beneath Gakkel ridge (Arctic ocean): abyssal peridotites spinel compositions," Chem. Geol. **182**, 227–235 (2002).
22. B. A. Bazylev and S. A. Silantyev, "Geodynamic interpretation of the subsolidus recrystallization of mantle spinel peridotites: 1. Mid-ocean ridges," Petrology **8** (3), 201–213 (2000).

*Translated by A. Girnis*